Journal of Photochemistry and Photobiology A: Chemistry 226 (2011) 42–50

Contents lists available at SciVerse ScienceDirect

Journal of Photochemistry and Photobiology A: Chemistry

journal homepage: www.elsevier.com/locate/jphotochem

Interfacial electron transfer dynamics and photovoltaic performance of TiO_2 and ZnO solar cells sensitized with Coumarin 343

Myrsini Giannouli, Mihalis Fakis*

Department of Physics, University of Patras, Patras 26504, Greece

ARTICLE INFO

Article history:
Received 17 May 2011
Received in revised form
19 September 2011
Accepted 12 October 2011
Available online 19 October 2011

Keywords:
Solar cell
Dye-sensitized
Electron transfer dynamics
Femtosecond spectroscopy
Coumarin 343

ABSTRACT

In this work, the photovoltaic performance and interfacial electron transfer (IET) dynamics of Coumarin 343 (C343) on ZnO and TiO_2 nanocrystalline semiconductors (sensitized films) were investigated using femtosecond upconversion spectroscopy. Inert Al_2O_3 nanostructured films were also used for comparison. In addition, electron transfer dynamics were studied in complete solar cells in the presence of a redox electrolyte in order to investigate the relation between electron transfer and solar cell performance. For the sensitized films, a more rapid IET was observed from C343 towards ZnO compared to TiO_2. An IET efficiency of 0.90 and 0.81 from C343 to ZnO and TiO_2 films respectively, was found at a transition corresponding to an emission wavelength of 480 nm. In the case of complete cells, electron transfer dynamics showed some retardation compared to the sensitized films. It is noteworthy that, in complete TiO_2 cells the injection dynamics were much faster than in ZnO ones, in contrast to the results obtained for sensitized semiconductor films. However, TiO_2 cells sensitized with C343 exhibited lower energy conversion efficiency than ZnO ones, indicating that faster injection is not always associated with better solar cell efficiency and that other factors, such as electron recombination, affect significantly the performance of the cells. Indeed, dark current measurements for ZnO and TiO_2 cells have shown that the recombination of the injected electrons with accepting sites in the electrolyte occurs more rapidly in TiO_2 cells, thus reducing their efficiency.

1. Introduction

Photovoltaic cells are considered a promising solution to the continuously growing energy problem by providing a sustainable and at the same time clean source of energy. Solar cells have improved in efficiency over the past decade and have experienced considerable commercial success. Commercially however, solar cells are still not competitive with conventional energy sources. Widespread usage of conventional silicon solar cells is still hampered by their high cost, which is mainly due to the high production costs of purified silicon. Dye-sensitized solar cells (DSSCs) present a relatively low-cost alternative to silicon solar cells. Over the past years, dye sensitized solar cells with highest efficiencies approximately 11% [1] have gained attention and considerable progress towards improving their performance has been made. These promising solar cells are developed using low-cost production processes and non-toxic materials, they are less sensitive to ambient temperature changes, they have good performance in low-light conditions and can be installed on flexible substrates [2]. Dye-sensitized solar cells however are still not commercially available in large volumes. Disadvantages such as the relatively low efficiency and stability of these cells, compared to silicon based solar cells, pose a hindrance to their commercialization.

In DSSCs, the conversion of visible light to electricity is achieved through the spectral sensitization of wide bandgap semiconductors. The sensitization of the semiconductors with dyes is required to improve their ability to absorb solar radiation and also to inject electrons into the conduction band of the semiconductor. The charge transfer mechanisms in a typical TiO_2 solar cell are shown in Fig. 1.

Incident light on the sensitized semiconductor surface is absorbed by dye molecules, leading to the excitation of the dye at a singlet state, as described by the following relationship:

$$S + h\nu \rightarrow S* \quad (1)$$

Excitation of the dye molecules is then followed by Interfacial Electron Transfer (IET) into the conduction band of the semiconductor [3–5]:

$$S* \rightarrow S^+ + e^- \quad \text{(semiconductor)} \quad (2)$$

The dye molecule has thus lost an electron and is left in its oxidized state. The positive charge remaining on the dye molecule is

* Corresponding author. Tel.: +30 2610996794.
E-mail address: fakis@upatras.gr (M. Fakis).

1010-6030/$ – see front matter © 2011 Elsevier B.V. All rights reserved.
doi:10.1016/j.jphotochem.2011.10.013

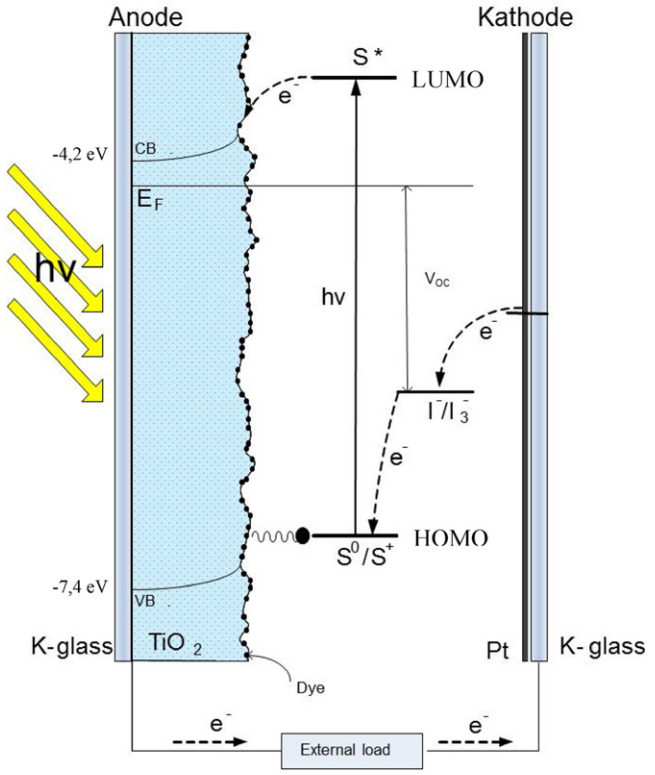

Fig. 1. Charge transfer mechanisms in a TiO_2 solar cell sensitized with C343.

transferred into the redox electrolyte, oxidizing the iodide into triiodide. The dye is thus regenerated in its original oxidation state as shown below:

$$S^+ + \frac{3}{2}I^- \rightarrow S + \frac{1}{2}I_3^- \quad (3)$$

The triiodide ions that were produced from the oxidization of iodide are transferred through the electrolyte to the cathode, where electrons from the platinum electrode reduce triiodide to iodide:

$$\frac{1}{2}I_3^- + e^-(\mathrm{Pt}) \rightarrow \frac{3}{2}I^- \quad (4)$$

IET from the dye sensitizer to the nanostructured semiconductor is the fundamental phenomenon that takes place in dye-sensitized solar cells. This phenomenon together with regeneration of the dye and transfer of the hole to the Pt back electrode compose the main charge cycle in a functional DSSC. However, other phenomena such as radiative and non-radiative decay, back electron transfer and electron recombination in the electrolyte affect the efficiency and properties of DSSCs [6]. Intense work is being devoted to the study of these processes, since controlling their rate is essential towards the optimization of DSSCs.

Femtosecond time resolved spectroscopy is a most valuable tool for evaluating the rate of each process and determining the relationship between carrier transport dynamics and solar cell performance. The majority of published works focuses on the dynamics of dye-sensitized semiconductor substrates [7–11]. It is now well-established that IET from the dye to the semiconductor occurs in the femtosecond timescale and is sometimes composed of two or three components with different time constants [7,9,12,13]. However, by examining complete solar cells we are able to study not only electron injection, but also other parameters, such as electron–hole recombination, dye regeneration by the electrolyte, as well as the effect of the electrolyte on the energetics of the semiconductor. This allows us to draw more comprehensive conclusions on how these factors affect electron transfer dynamics and the overall performance of DSSCs. Several recently published works focus on the study of electron dynamics in complete, functional DSSCs [14–17]. In these works it was reported that IET occurs on a much longer timeframe than in sensitized films, specifically on tens to hundreds of picoseconds. Combining these dynamic measurements with device performance characterisation, it was concluded that an ultrafast IET is not required for an efficient DSSC, as long it remains 10–100 times faster than radiative recombination (which is typically on the tens of ns timescale).

The most efficient sensitizers for wide bandgap semiconductors are metallo-organic ruthenium complexes due to their high charge-transfer efficiency to TiO_2 and light absorption in the visible spectrum [18]. Solar cells sensitized with such dyes not only yield high efficiencies, but also present improved stability compared to cells sensitized with simple organic molecules [19]. Ruthenium complexes however, are expensive and their use renders the resulting solar cells costly. Moreover, several simple organic dyes, and especially xanthene dyes (Eosin Y, Rose Bengal, etc.), yield efficiencies comparable to those achieved with ruthenium complexes when used for sensitizing ZnO films [20]. These dyes are inexpensive [21] and do not rely on the availability of precious metals such as ruthenium [22]. They also have high extinction coefficients and their molecular structures contain adequate anchoring groups to be chemically adsorbed onto the oxide surface. Coumarin dyes also constitute a class of organic dyes capable to be used as sensitizers in DSSCs [23,24]. Especially, coumarin 343 (C343) is considered ideal for studying IET dynamics [25–30]. Although, the IET dynamics of C343 on TiO_2 have been well studied, the dynamics of C343 on ZnO have not been thoroughly investigated [25]. Additionally, the IET dynamics have only been studied in C343-sensitized semiconductor interfaces and not in complete devices.

In this work, the photovoltaic performance and IET dynamics, in the femtosecond regime, of C343 on TiO_2 and ZnO nanostructured semiconductors are studied and compared. The decay dynamics of C343 are also studied on an inert oxide such as Al_2O_3, used as reference. It is found that IET occurs faster and more efficiently on ZnO than on TiO_2 substrates. This is consistent with the relative positions of the conduction bands of ZnO and TiO_2 and the LUMO of C343. Finally, in order to relate the injection process with cell performance, IET dynamics are studied in complete DSSCs using C343 as a sensitizer, ZnO and TiO_2 as semiconductors and a redox electrolyte.

2. Materials and methods

2.1. Preparation of dye-sensitized solar cells

Nanostructured ZnO, TiO_2 and Al_2O_3 films were prepared as described in [31]. The films were deposited on transparent conductive oxide (TCO) glass surfaces, which were coated with a fluorine doped tin oxide layer (SnO_2:F sheet resistance of 16.7 Ω/sq, 80% transmittance in the visible, 0.38 cm glass thickness). Commercial ZnO, TiO_2 and Al_2O_3 nanopowder was used to create a colloidal paste that was spread on the glass surface. The nanopowder was mixed with a small amount of distilled water (different for each semiconductor mixture prepared) containing acetyl acetone (10% v/v) [32,33]. Acetyl acetone was used in the mixture in order to prevent the coagulation of nanoparticles and improve the porosity of the film [34]. The paste was diluted further in order to reduce its viscosity, by addition of distilled water under continuous stirring. A small amount of Triton X-100 was added to the mixture to reduce surface tension and enable even spreading of the paste [35,36]. The specific amount of each material used for the preparation of the three different pastes is shown in Table 1.

Table 1
Composition of ZnO, TiO_2 and Al_2O_3 pastes.

	Powder (g)	Acetyl acetone (ml)	Water (ml)	Triton X-100 (drops)
TiO_2	3.0	1.0	5.0	2
ZnO	3.0	0.5	7.0	2
Al_2O_3	3.0	0.5	4.0	2

The paste was spread on the conductive glass substrates via a doctor blade technique. After air drying, the electrodes were annealed for 30 min at 450 °C in air. Sintering enhances the electrical contact between the nanoparticles as well as between the nanoparticles and the conductive substrate [37]. Small cracks sometimes appear on the surface of TiO_2 films, during the drying process, before sintering. Film thickness also plays an important role in the formation of cracks, as thicker films tend to have more cracks. It has been observed that the presence of cracks on the surface of the films results to a decrease in the efficiency of the cells. This occurs mainly because the formation of cracks on the film's surface reduces electrical contact between TiO_2 nanoparticles. Also, if the cracks reach to the conducting substrate, electron recombination is increased due to contact of the electrolyte with the conducting substrate. For the above reasons, TiO_2 films in particular, were developed via a process that limits the formation of cracks on the surface of the films [38].

After preparation, ZnO, TiO_2 and Al_2O_3 films were sensitized with C343 which is a well-known sensitizer and it is also useful as a model dye for the study of IET dynamics. Coating of the semiconductor surface with the dye was conducted by soaking the film in a solution of the dye in methanol (0.01 M) for at least 12 h. The soaking time of the films was optimized according to the film thickness and afterwards any excess dye was washed off using a small amount of methanol.

The type of electrolyte used plays a fundamental part in the conversion efficiency of the solar cell. For the purpose of this study an electrolyte containing 0.3 M potassium iodide and 0.03 M iodine in propylene carbonate (PC) was used.

Counter electrodes were also prepared through thermal decomposition of a 5 mM hexachloroplatinic acid in isopropanol solution. The solution was also spread on SnO_2:F covered conductive glass substrates (K-glass). The sensitized semiconductor electrode and the counter electrode were then assembled as a sandwich-type cell and sealed together with silicon. Electrical contacts were made on both electrodes using conductive adhesive copper tape. The electrolyte was inserted in the cell with a syringe through a small aperture, which was then sealed with silicon.

2.2. Property characterisation of DSSCs

The solar cells prepared as described above were illuminated with a 50 W halogen lamp, which provided illumination intensity equal to 708 W/m^2. Current–Voltage (I–V) curves of the cells were obtained using an AMEL Function Generator directly connected to a PC. The most important characteristics of the solar cells, such as the open circuit voltage, the short circuit current, the fill factor and the efficiency of the cell, can be obtained from these I–V curves. The aforementioned properties were measured at regular intervals after the preparation of the cells in order to evaluate the stability of the devices over time. Dark current measurements were also conducted for ZnO and TiO_2 cells by applying bias voltage equal to the open circuit voltage. Dark current arises when triiodide ions from the electrolyte draw electrons from the semiconductor, reducing the triiodide to iodide. Since electrons are removed from the semiconductor, the overall current produced in the photovoltaic cell is reduced.

Scanning Electron Microscope (SEM) images were obtained (SEM, JEOL 6300) in order to examine the morphology of the films and to determine the average size of the particles. Film thickness was measured with a stylus XP-1 Ambios Technology profilometer. Step height measurements between film-coated and uncoated areas were conducted to determine film thickness. The stylus profilometer was also used to assess the surface morphology and roughness of the films.

2.3. Steady state spectroscopy

The absorption and fluorescence spectra of C343 in various environments have been measured using a Perkin Elmer Lambda 650 UV/VIS Spectrometer and a Perkin Elmer LS45 luminescence spectrometer respectively.

2.4. Time resolved spectroscopy

C343 emits fluorescence at the blue-green spectral region and the dynamics were detected at three wavelengths across its fluorescence spectrum, i.e. at 450, 480 and 520 nm. Femtosecond time resolved fluorescence upconversion spectroscopy was used for this reason. This technique provides information on the injection dynamics from the dye towards the semiconductor excluding complex decay components associated with dye cations and injected electrons [8,26,39,40]. The system has been described in detail elsewhere [41,42]. The laser source was a mode-locked Ti:Sapphire femtosecond laser emitting 80 fs laser pulses at 800 nm with 82 MHz repetition rate. The second harmonic, at 400 nm, was generated in a 0.5 mm Beta Barium Borate (BBO) crystal and was used for the excitation of the samples, while the remaining fundamental beam was used as a gate beam. The excitation power was typically below 5 mW and the samples were placed in a rotating holder in order to avoid thermal degradation. The fluorescence of the samples was collected and focused on a second BBO crystal (0.5 mm) together with the gate beam. The two beams overlapped both spatially and temporally on the crystal to generate an upconversion beam via type I phase matching. This beam passed through appropriate filters and a monochromator and it was detected through a photomultiplier as a function of the temporal delay between the gate and the excitation pulses. The temporal resolution of the technique was ~150 fs and the decays were taken under magic angle conditions.

3. Results and discussion

3.1. Semiconductor film morphology

As mentioned above, the morphology of the ZnO films was determined using Scanning Electron Microscope images of the semiconductor films. Fig. 2 shows examples of TiO_2 and ZnO films. A TiO_2 film is presented in Fig. 2a, showing, in general, an even surface of TiO_2 nanoparticles. Small cracks, such as the one appearing near the bottom end of this figure, appeared on the surface of very few of the films. As mentioned above, these cracks were formed in TiO_2 films during the drying process, before sintering.

Fig. 2b shows a SEM image of a typical ZnO film developed during this study. It can be observed that the films have high porosity and consist of a fairly uniform layer of ZnO nanoparticles. Particle size for both TiO_2 and ZnO films was found to be in the range of 60–80 nm.

The morphology of the films was further investigated through stylus profilometer measurements. Fig. 3 shows the variation in thickness and morphology of a ZnO and a TiO_2 film. Both samples are representative of the films prepared throughout the study. From Fig. 3 it can be observed that the ZnO film is more uniform than the

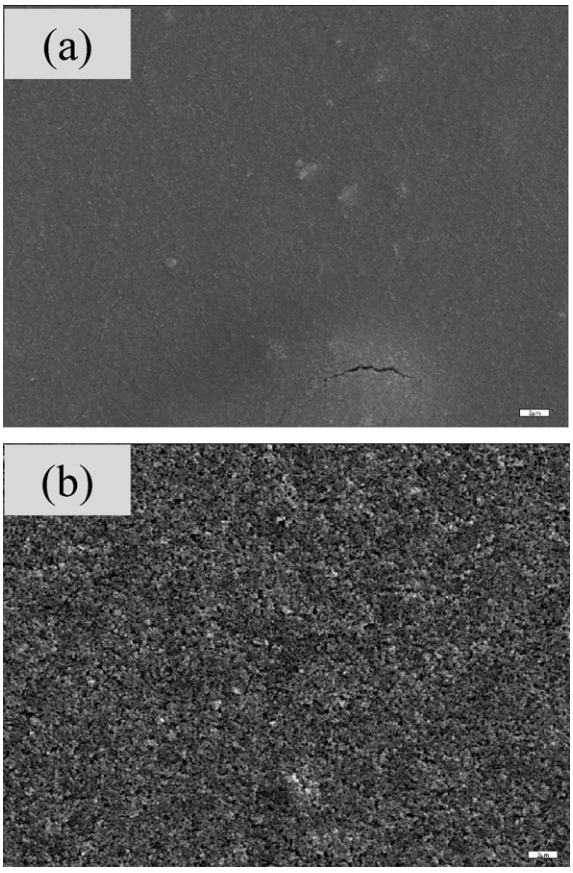

Fig. 2. SEM images of semiconductor films (a) TiO_2 and (b) ZnO. The bars on the bottom right corners are equal to 2 μm.

TiO_2 film as was also observed from the SEM images. The irregularities observed in the profiles of the TiO_2 film represent nanoparticle aggregates and small cracks, that were formed in some TiO_2 films during sintering.

The thickness of the films prepared was also determined through stylus profilometer measurements and was found to range from 8 to 11 μm. Since the thickness of the semiconductor films affects cell performance considerably [43,44], the comparisons of cell performance that are presented in the following sections were conducted between films of similar thickness (difference of film thickness less than 0.5 μm).

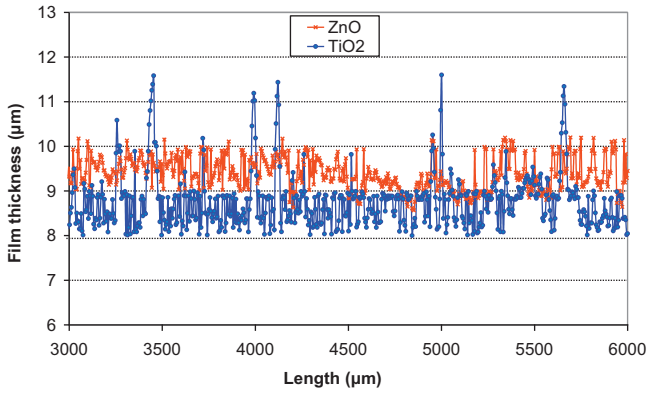

Fig. 3. Morphology of a ZnO and a TiO_2 film.

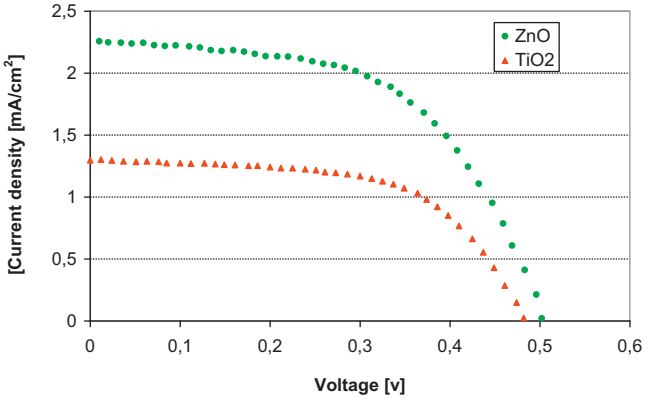

Fig. 4. Current density vs. Voltage for a ZnO and a TiO_2 cell sensitized with C343.

3.2. Solar cell efficiency

In general, TiO_2 cells sensitized with metal complexes tend to yield higher efficiencies than ZnO ones due to the disadvantages of using these complexes with ZnO. On the other hand, ZnO DSSCs with simple organic dyes tend to be more efficient than TiO_2 cells [45]. Fig. 4 shows the Current–Voltage characteristics of ZnO and TiO_2 cells sensitized with C343. These results are representative of the majority of the results obtained during the study. ZnO cells sensitized with C343 yielded higher values of both the short-circuit current and the open-circuit voltage than TiO_2 cells. As a result, ZnO cells yielded higher efficiency values than corresponding TiO_2 ones. Overall, the efficiency of ZnO cells sensitized with C343 was found to be 39–53% higher than that of TiO_2 cells. The uncertainty in these results originates from differences in the structure and assembly of the various solar cells, mainly related to the thickness and the uniformity of the semiconductor films [31]. Al_2O_3 solar cells sensitized with C343 were also prepared and tested for comparison. These cells did not display photovoltaic properties indicating that Al_2O_3 films can be used as inert reference samples.

The main parameters that characterize solar cell performance, i.e. the open-circuit voltage (V_{oc}), the short-circuit current (I_{sc}), the fill factor (FF) and the efficiency (η) of the cells, are summarized in Table 2. The uncertainty in these results is due to small differences in the cells prepared throughout this study, as mentioned above.

3.3. Device stability

The stability of the solar cells also plays a very important role in assessing their overall performance. The efficiency of DSSCs tends to decrease considerably with time mainly due to the degradation of the dye sensitizer [46].

Fig. 5 shows the evolution of cell efficiency over a 30 day period for typical ZnO and TiO_2 cells. The efficiency of ZnO solar cells is higher than that of TiO_2 cells, but drops more rapidly with time, while TiO_2 cells maintain relatively high efficiencies for some time after cell preparation. Overall, it was observed that ZnO cells experience a drop of 50–70% in their efficiency, within 30 days after preparation, while TiO_2 cells lose approximately 30–40% of their original efficiency during the same time.

Table 2
Photovoltaic properties of ZnO and TiO_2 cells.

	J_{sc} (mA/cm$_2$)	V_{oc} (mV)	η (%)	FF
TiO_2	1.31 (±0.07)	0.48 (±0.02)	0.51 (±0.05)	0.54 (±0.03)
ZnO	2.3 (±0.08)	0.51 (±0.02)	0.92 (±0.03)	0.59 (±0.02)

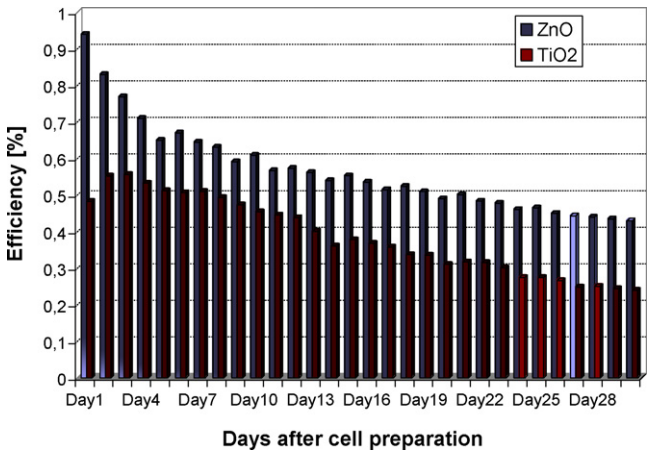

Fig. 5. Evolution of cell efficiency over a 30 day period for a ZnO and a TiO_2 solar cell sensitized with Coumarin 343.

TiO_2 cells yield their highest efficiencies at the 2nd or 3rd day after preparation due to gradual permeation of the electrolyte [47]. Cell efficiency follows the trend of the short-circuit current density, which reaches its maximum value on the 2nd or 3rd day after cell preparation and then gradually decreases. On the other hand, the value of the open-circuit voltage increases slightly with time, but does not vary as much as the value of the current and cannot compensate for the large drop in the current. The gradual decrease in the current that was observed after the 3rd day from cell preparation is mainly due to dye desorption and degradation. Many organic dyes undergo degradation when they are adsorbed on the surface of a semiconductor such as the TiO_2, which can cause catalytic photodegradation. In addition, reactive oxygen species are formed with time, which react with oxidized dye molecules under visible or ultraviolet light irradiation in the presence of TiO_2 particles [48,49]. As a result, the number of oxidized dye molecules is reduced. Dye degradation depends also on the adsorption sites [46] and constitutes a major problem not only for the simple organic dyes, but also for the high efficient metal complexes [50].

For ZnO films in particular, protons originating from the dye break up Zn surface atoms [51]. These Zn atoms then react with the protons from the dye, forming Zn^{+2}/dye complexes:

$$ZnO + 2H^+ \rightarrow Zn^{2+} + H_2O \quad (5)$$

The above reaction leads to the formation of inactive dye molecules which limit charge carrier injection and reduce the efficiency of the cells. For this reason, TiO_2 cells display higher stability than ZnO cells. The dissolution of ZnO depends on a number of factors, such as the dye concentration, the sensitization time and the pH of the dye solution [52].

3.4. Steady state absorption and fluorescence spectra

The steady state absorption spectra of C343 sensitized films and cells are shown in Fig. 6a. The absorption spectrum of C343 in MeOH solution is shown in the inset of Fig. 6a for comparison. All steady state spectroscopic parameters are summarized in Table 3. The absorption spectrum of C343 in MeOH exhibits a peak at 445 nm while the spectra of C343 on the sensitized films are red shifted, exhibiting peaks at 457–469 nm and they are also significantly broadened. The red shift is due to the adsorption of the dye and the subsequent formation of *J* – aggregates on the surface of the semiconductor [31]. In complete cells, the absorption maxima exhibit only a slight shift of 6–9 nm, compared to the sensitized films, due to the presence of the electrolyte. A new feature in the absorption spectra of complete cells is the broader tail towards the

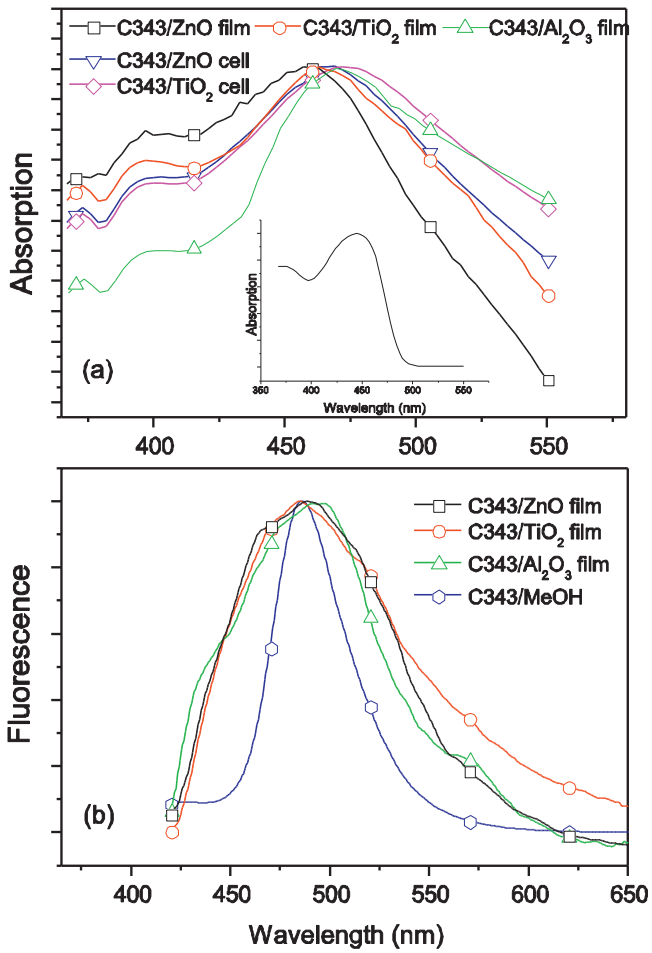

Fig. 6. (a) Absorption spectra of C343 on TiO_2, ZnO and Al_2O_3 films and in TiO_2 and ZnO complete cells. The inset shows the absorption spectrum of C343 in MeOH solution. (b) Fluorescence spectra of C343 on TiO_2, ZnO and Al_2O_3 sensitized films. The spectrum of C343 in MeOH solution is also shown.

red edge, compared to the spectra of the sensitized films, indicating a small contribution in the absorption from the electrolyte and the platinum electrode. In the case of the complete cells, the reflectance of the platinum electrode was also measured and taken into account in determining the final absorption spectrum.

In Fig. 6b, the fluorescence spectra of C343 sensitized films are shown together with the spectrum of C343 in MeOH for comparison. The fluorescence spectra were measured using an excitation wavelength of 400 nm. Fluorescence spectra in complete cells could not be measured accurately because of intense attenuation of the emitted fluorescence mainly due to absorption from the electrolyte and Pt electrode, scattering and internal reflections in the cell. The spectra of the sensitized TiO_2 and ZnO films exhibit peaks at 485 and 488 nm respectively, showing an almost negligible shift compared to the spectrum of C343 in solution, exhibiting a peak at 486 nm. The sensitized Al_2O_3 film shows a red-shifted peak at 497 nm indicating a more pronounced aggregation effect compared to the TiO_2 and ZnO films. Finally, in agreement with the absorption spectra, the fluorescence spectra in films are significantly broadened, towards both short and long wavelengths, compared to the spectrum in the dye solution.

3.5. Dynamics of C343 on sensitized films

The fluorescence dynamics of C343 were studied on TiO_2 and ZnO semiconductors, as well as on Al_2O_3, which was used as a

Table 3
Steady state absorption and fluorescence properties of C343 on TiO_2, ZnO and Al_2O_3 sensitized films as well as in MeOH solution.

C343 in	MeOH	TiO_2 film	ZnO film	Al_2O_3 film	TiO_2 cell	ZnO cell
$\lambda_{abs\ max}$ (nm)	445	463	457	469	472	463
$\lambda_{fuor\ max}$ (nm)	486	485	488	497	–	–

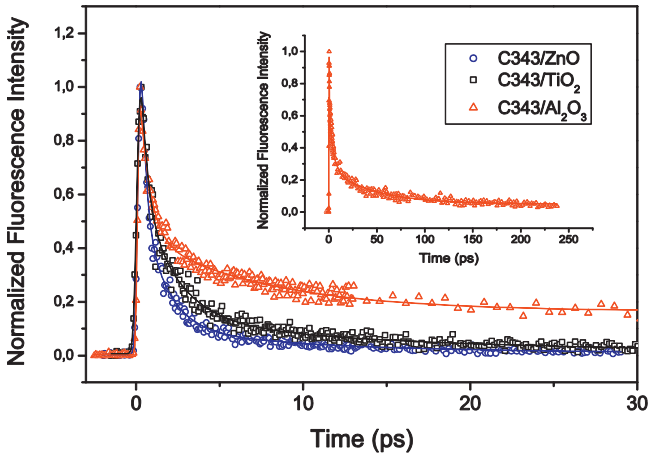

Fig. 7. Decay dynamics of C343 on TiO_2, ZnO and Al_2O_3 substrates detected at an emission wavelength of 480 nm. The inset shows the dynamics on Al_2O_3 at long timescale.

Table 4
Decay parameters of C343 on ZnO at emission wavelengths of 450, 480 and 520 nm.

λ_{det} (nm)	C343/ZnO				
	τ_1 (ps)	τ_2 (ps)	τ_3 (ps)	$\langle\tau\rangle$ (ps)	Φ_{IET}
450	0.25 (0.83)	1.7 (0.12)	7.9 (0.05)	0.8	0.50
480	0.24 (0.64)	1.4 (0.30)	9.0 (0.06)	1.1	0.90
520	0.53 (0.67)	3.0 (0.26)	29 (0.07)	3.2	0.86

Table 5
Decay parameters of C343 on TiO_2 at emission wavelengths of 450, 480 and 520 nm.

λ_{det} (nm)	C343/TiO_2				
	τ_1 (ps)	τ_2 (ps)	τ_3 (ps)	$\langle\tau\rangle$ (ps)	Φ_{IET}
450	0.17 (0.35)	0.52 (0.45)	3.6 (0.20)	1.0	0.38
480	0.36 (0.55)	2.0 (0.36)	13 (0.09)	2.1	0.81
520	0.30 (0.62)	3.3 (0.28)	40 (0.10)	5.1	0.78

reference substrate. The results obtained by detecting the fluorescence at 480 nm, which is very close to the wavelength of the fluorescence maximum (Fig. 6b), are shown in Fig. 7. In the inset of Fig. 7, the dynamics of C343 on Al_2O_3 are shown on a long timescale. The similarity of the fluorescence spectra and the coincidence of the fluorescence maxima in all sensitized films (Fig. 6b), confirm that the same energy of the excited state is probed in each case. The decays in all substrates were fitted with a three-exponential decay function taking into account the convolution with the Instrument Response Function [53]. All fitting parameters including time constants and pre-exponential factors are summarized in Tables 4–6.

Table 6
Decay parameters of C343 on Al_2O_3 at emission wavelengths of 450, 480 and 520 nm.

λ_{det} (nm)	C343/Al_2O_3				
	τ_1 (ps)	τ_2 (ps)	τ_3 (ps)	$\langle\tau\rangle$ (ps)	Φ_{IET}
450	0.36 (0.67)	2.0 (0.28)	17 (0.05)	1.6	–
480	0.42 (0.46)	4.3 (0.35)	47 (0.19)	11	–
520	0.63 (0.51)	5.9 (0.31)	116 (0.18)	23	–

In Al_2O_3 the dynamics exhibit the slowest decay among the three substrates used. This occurs because, in Al_2O_3, IET is energetically not favourable and the dynamics probe only the fundamental radiative and non-radiative mechanisms of the dye. In this case, aggregation induced non-radiative decay, associated with intermolecular energy transfer from isolated molecules to energetically lower lying non-fluorescent aggregate species, is expected to play a significant role. This occurs because there is neither liquid solvent nor solid matrix to prevent molecular stacking and therefore the molecules approach each other to form aggregate clusters. In the case of ZnO and TiO_2 semiconductors, the dynamics become faster than in Al_2O_3 since apart from radiative and non-radiative decay, electron injection from C343 to the conduction band of the semiconductors also takes place, quenching the fluorescence. It is noted that the dynamics on ZnO are faster than on TiO_2. Considering that the radiative and non-radiative decay mechanisms of the Coumarin dye are identical, irrespective whether it is adsorbed on TiO_2 or ZnO, the shortening of the dynamics on ZnO indicates a more rapid electron injection process on this semiconductor.

Fig. 8 shows the dynamics of C343 on TiO_2, ZnO and Al_2O_3 at three different wavelengths across the fluorescence spectrum. The detailed fitting parameters are also presented in Tables 4–6. In all cases, three decay components were used to fit the data. This multiexponential decay of C343 on the nanocrystalline semiconductors TiO_2 and ZnO indicates a multiphasic injection process which has also been reported in previous works [7,9,12,53,54] and is mainly

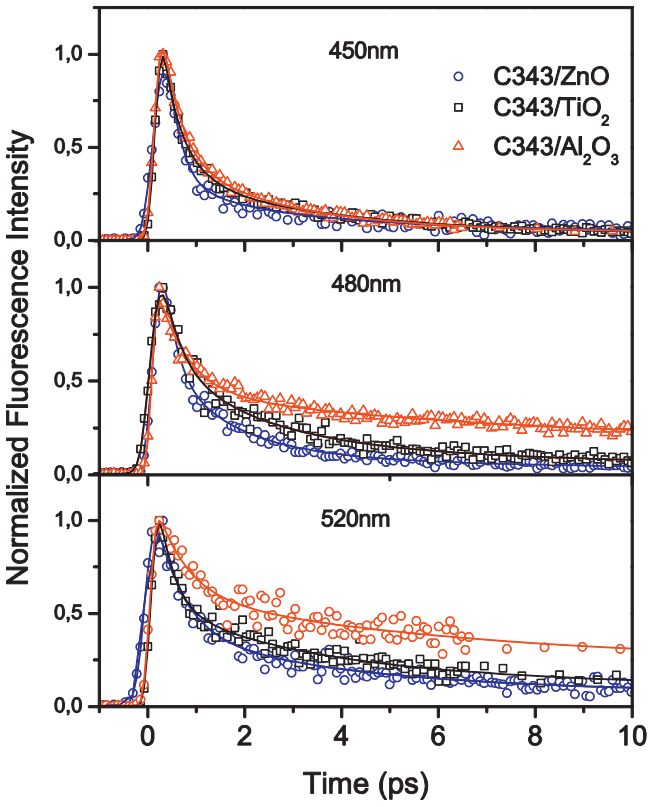

Fig. 8. Decay dynamics of C343 on TiO_2, ZnO and Al_2O_3 substrates detected at emission wavelengths of 450, 480 and 520 nm.

due to the following factors: (i) the inhomogeneity of the sensitized films. The adsorption of dye molecules on the surface of the semiconductor films leads to the formation of molecular species with various conformations and geometries injecting electrons at different rates. For example, molecular aggregates existing on the oxide surface may also inject electrons to the semiconductor but at a slower rate than the adsorbed dye molecules, (ii) the fact that electrons are injected from various vibronic sublevels of the dye's excited state towards a continuum of states, with different energies, in the semiconductor's conduction band. For example, electron injection takes place from the energetically higher and lower vibronic sublevels of the dye's singlet state as well as from the triplet state (in transition metal based dyes). As the energy of the injection state is lowered, the injection becomes slower, leading to a distribution of injection times.

Using the equation $\langle\tau\rangle = \sum_{i=1}^{N} A_i\tau_i$ where A_i are the pre-exponential factors which satisfy the condition $\sum_{i=1}^{N} A_i = 1$, the amplitude averaged decay times were calculated and are also shown in Tables 4–6 for C343 on ZnO, TiO_2 and Al_2O_3 respectively. The IET quantum yield in each semiconductor and at each transition wavelength was calculated through the equation $\Phi_{IET,x} = 1 - \frac{\langle\tau_x\rangle}{\langle\tau_{Al_2O_3}\rangle}$ [39,53], where x denotes the semiconductor, i.e. ZnO or TiO_2. In the above equation, it is assumed that apart from IET, all other decay mechanisms of C343 on TiO_2, ZnO and on Al_2O_3 are the same. Finally, the results obtained are $\Phi_{IET,ZnO} = 0.50$ and $\Phi_{IET,TiO_2} = 0.38$ at 450 nm, $\Phi_{IET,ZnO} = 0.90$ and $\Phi_{IET,TiO_2} = 0.81$ at 480 nm and $\Phi_{IET,ZnO} = 0.86$ and $\Phi_{IET,TiO_2} = 0.78$ at 520 nm (Tables 4 and 5). By considering the results of the electron transfer quantum yields, the following conclusions are drawn.

The electron transfer from C343 to ZnO is more efficient than to TiO_2 in all wavelengths. This is explained by taking into account the different energy of the conduction bands of ZnO and TiO_2. The conduction band of ZnO (−4.5 eV) is lower than that of TiO_2 (−4.2 eV), thus increasing the free energy difference between the dye's LUMO and the conduction band edge (driving force). This favours more efficient electron injection by increasing the density of accepting states in the semiconductor. However, the difference between the conduction band energy of the semiconductor and the LUMO level of the dye is not the only factor that influences electron transfer rate and short circuit current. The electronic nature of the conduction band and the electronic coupling with the dye also determine the transfer of electrons [54]. Although the faster electron transfer dynamics from C343 to ZnO than to TiO_2 agree with the better photovoltaic performance of the ZnO cells compared to the TiO_2 ones, they cannot be directly associated with it. Accurate conclusions can only be drawn by studying the injection dynamics in complete solar cells as it will be discussed below.

In addition, the IET quantum yield is small at the transition corresponding to an emission wavelength of 450 nm, becomes high at 480 nm and then is reduced again at 520 nm. The small electron injection efficiency at the emission wavelength of 450 nm is directly evident by the similarity of the decay curves in ZnO, TiO_2 and Al_2O_3. When the short wavelength region is detected, the electrons occupying the highest vibronic sublevels of the first singlet excited state S_1 are probed. These electrons decay by (i) vibronic relaxation to lower energy vibronic sublevels, (ii) relaxation towards fluorescent traps and aggregates as well as by (iii) electron injection to the conduction band of the semiconductor. These decay channels kinetically compete with each other since they occur on a similar timescale. Therefore, the amount of electrons participating in the injection process from the energetically higher vibronic sublevels is reduced. At the intermediate emission wavelength (480 nm),

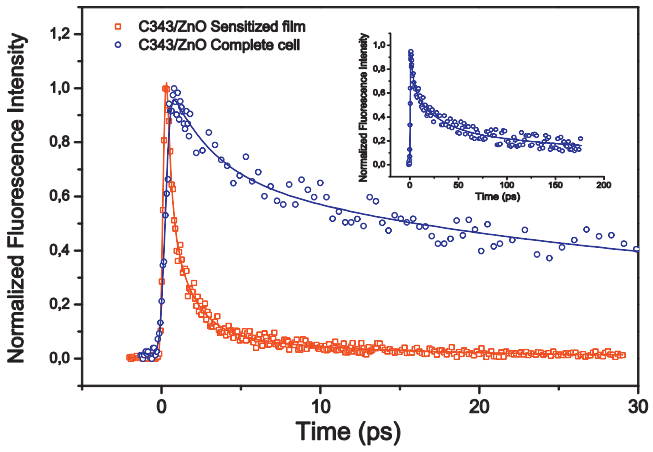

Fig. 9. Dynamics of C343, detected at an emission wavelength of 480 nm, in complete ZnO solar cells. The dynamics of a ZnO film sensitized with C343 is also shown for comparison. The inset shows the decay in the complete cell at long timescale.

which is close to the maximum of the fluorescence spectrum of C343, the electron transfer to the semiconductor mainly competes with radiative decay. Since radiative decay occurs on the nanosecond timescale while electron transfer on the 100 fs one, it is to be expected that IET efficiency would become highest at this wavelength. Finally, at the longest detected emission wavelength, only the species that have relaxed to the lower vibronic sublevels are probed. Thus, the excess energy of the emitting excited state species is reduced and the energy difference between them and the conduction band becomes minimum. Consequently, the density of states of electron-accepting energy levels in the semiconductor is also reduced leading to a less favourable electron injection process. For this reason, the IET quantum yield is reduced at long wavelengths, although its value remains relatively high.

3.6. Dynamics of C343 in complete solar cells

Figs. 9 and 10 show the fluorescence decays of C343 in complete DSSCs using ZnO and TiO_2 nanostructured semiconductors respectively. The redox electrolyte and back electrode were fabricated according to the procedures described in the experimental section. The dynamics were detected at an emission wavelength of 480 nm, being very close to the fluorescence maxima of C343 sensitized

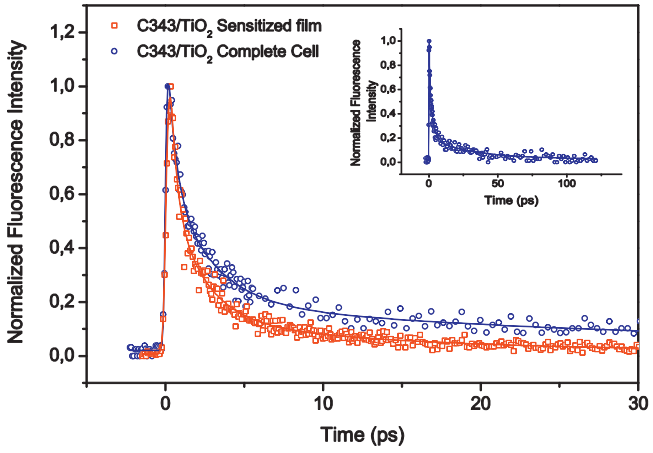

Fig. 10. Dynamics of C343, detected at an emission wavelength of 480 nm, in complete TiO_2 solar cells. The dynamics of a TiO_2 film sensitized with C343 is also shown for comparison. The inset shows the decay in the complete cell at long timescale.

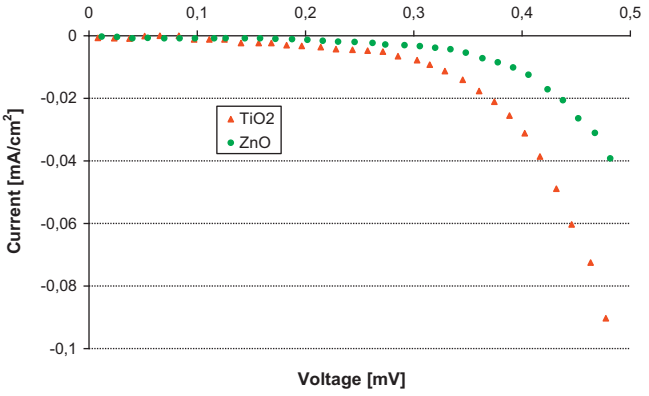

Fig. 11. Dark Current–Voltage characteristics of a ZnO and a TiO_2 cell sensitized with C343.

films. The decays obtained by simple sensitized films (C343/ZnO and C343/TiO_2) are also shown for comparison.

It is apparent from Figs. 9 and 10, that the decays of C343 in complete devices are slower than in sensitized films. Specifically, three-exponential decay functions are used to fit the data with $\tau_1 = 2.7$ ps (0.32), $\tau_2 = 24$ ps (0.39) and $\tau_3 = 230$ ps (0.29) for ZnO and $\tau_1 = 0.5$ ps (0.47), $\tau_2 = 2.8$ ps (0.39) and $\tau_3 = 32$ ps (0.14) for TiO_2. Thus, the average decay times are 77 ps and 7 ps for ZnO and TiO_2 cells respectively. This means that the injection dynamics experience a 69 times retardation in the case of ZnO cells while in the case of TiO_2 there is only a 3.3 times retardation.

The electron injection dynamics in complete DSSCs have been studied in the past using time resolved fluorescence, transient absorption and time resolved THz spectroscopy [14–17]. The previous studies have been restricted to Ru-based sensitizers while the semiconductors used were TiO_2 and SnO_2. A similar dynamic study, performed on organic dyes adsorbed on ZnO semiconductor, has not been published to the best of our knowledge. A retardation in injection dynamics in both TiO_2 and SnO_2 cells compared to sensitized semiconductor films was reported in all previous works, in agreement with our own findings. The retardation was attributed to a shift of the semiconductor conduction band to more positive potentials due to the presence of the electrolyte. This shift reduces the density of acceptor states, thus retarding electron injection. In our case, retardation in injection dynamics is observed for both ZnO and TiO_2 solar cells, although in the case of ZnO, the retardation is much more intense, indicating that the presence of the electrolyte produces a similar, yet stronger, effect on ZnO than on TiO_2. As in previous works, the retardation in the injection dynamics is likely caused by a positive shift of the conduction band of the two semiconductors and in this case, the shift would be larger in ZnO than in TiO_2.

In order to correlate the injection dynamics with device performance, we have to note that although in ZnO cells the injection dynamics are slower than in TiO_2 cells, the ZnO devices exhibit better photovoltaic performance. The faster dynamics observed in TiO_2 cells are expected to yield higher values of short circuit current density. However, the opposite is observed. This is mainly due to the recombination of the injected electrons with accepting ions in the electrolyte (i.e. I_3^-), which occurs more efficiently in TiO_2 cells sensitized with C343 than in ZnO ones. The more efficient recombination in TiO_2 cells was confirmed through dark current measurements of ZnO and TiO_2 cells sensitized with C343. The results of these measurements are shown in Fig. 11. From this figure it can be observed that TiO_2 cells have considerably higher dark current than corresponding ZnO cells, indicating more efficient electron recombination with accepting states in the electrolyte. A similar behaviour has also been reported for acriflavine-sensitized TiO_2 and ZnO nanocrystalline films [45]. In the case of sensitization with acriflavine, the photocurrent was significantly higher in ZnO than in TiO_2 cells, although the injection from this dye towards ZnO was less efficient than towards TiO_2. This is in agreement with our own results for C343. The above findings indicate that injection dynamics do not always determine device efficiency, i.e. faster injection dynamics are not always associated with better photovoltaic performance. A combination of various processes such as back transfer, electron transport and electron collection at the electrode need to be optimized to achieve high efficiency values.

4. Conclusions

The aim of this work was to study the electron transfer dynamics in ZnO and TiO_2 semiconductor films and in complete solar cells sensitized with the organic dye Coumarin 343. Femtosecond upconversion spectroscopy was used in order to examine these processes. The photovoltaic performance of TiO_2 and ZnO solar cells sensitized with C343 was also determined and its relationship with the observed dynamics was investigated. It was found that ZnO cells achieve a better photovoltaic performance than TiO_2 ones. For ZnO and TiO_2 films sensitized with C343 it was found that electron injection occurs faster on ZnO than on TiO_2 substrates. This is consistent with the lower energy of the conduction band of ZnO than TiO_2. By analysing the dynamic data, an IET efficiency of 0.90 and 0.81 was found in ZnO and TiO_2 respectively at a transition of 480 nm. In the case of complete DSSCs prepared using both ZnO and TiO_2 semiconductors, a retardation in the injection dynamics was observed, compared to the sensitized films, in agreement with previous reports. In TiO_2 complete cells, the injection dynamics were faster than in ZnO ones although the TiO_2 cells have shown lower efficiency. This indicates that fast injection dynamics are not always sufficient to achieve high photovoltaic efficiency and that other factors, such as electron–hole recombination in the electrolyte, considerably affect the performance of DSSCs. Dark current measurements conducted for both ZnO and TiO_2 cells sensitized with C343 indicate that the recombination of the injected electrons with acceptors in the electrolyte occurs more efficiently in TiO_2 cells than in ZnO ones. The more efficient carrier recombination in TiO_2 cells is responsible for their lower efficiency compared to ZnO cells, even though electron injection rates for TiO_2 cells sensitized with C343 are higher than those of corresponding ZnO ones.

References

[1] F. Gao, Y. Wang, J. Zhang, D. Shi, M. Wang, R. Humphry-Baker, P. Wang, S. Zakeeruddin, M. Grätzel, J. Am. Chem. Soc. 130 (2008) 10720–10728.
[2] M. Grätzel, J. Photochem. Photobiol. A: Chem. 164 (2004) 3–14.
[3] M. Matsumura, Y. Nomura, H.B. Tsubomura, Chem. Soc. Jpn. 50 (1977) 2533–2537.
[4] J. Zhao, C. Chen, W. Ma, Top. Catal. 35 (2005) 269–278.
[5] R.C. Nelson, J. Phys. Chem. 69 (1965) 714–718.
[6] S. Caramori, V. Cristino, R. Boaretto, R. Argazzi, C. Bignozzi, A. Di Carlo, Int. J. Photoenergy (2010) 1–16.
[7] G. Benkö, J. Kallioinen, J.E.I. Korppi-Tommola, A.P. Yartsev, V. Sundström, J. Am. Chem. Soc. 124 (2002) 489–493.
[8] M. Ziolek, I. Tacchini, M.T. Martinez, X. Yang, L. Sun, A. Douhal, Phys. Chem. Chem. Phys. 13 (2011) 4032–4044.
[9] Y. Tachibana, I.V. Rubtsov, I. Montanari, K. Yoshihara, D.R. Klug, J.R. Durrant, J. Photochem. Photobiol. A: Chem. 142 (2001) 215–220.
[10] M.C. Rath, D.K. Palit, T. Mukherjee, H.N. Ghosh, J. Photochem. Photobiol. A: Chem. 204 (2009) 209–216.
[11] L. Luo, C.-F. Lo, C.-L. Lin, I.-J. Chang, E.D.W. Diau, J. Phys. Chem. B 110 (2006) 410–419.
[12] J.B. Asbury, N.A. Anderson, E. Hao, X. Ai, T. Lian, J. Phys. Chem. B 107 (2003) 7376–7386.
[13] G. Benkö, M. Hilgendorff, A.P. Yartsev, V. Sundström, J. Phys. Chem. B 105 (2001) 967–974.
[14] J.J.H. Pijpers, R. Ulbright, S. Derossi, J.N.H. Reek, M. Bonn, J. Phys. Chem. C 115 (2011) 2578–2584.
[15] S.E. Koops, J.R. Durrant, Inorg. Chim. Acta 361 (2008) 663–670.

[16] S.A. Haque, E. Palomares, B.M. Cho, A.N.M. Green, N. Hirata, D.R. Klug, J.R. Durrant, J. Am. Chem. Soc. 127 (2005) 3456–3462.
[17] S.E. Koops, B.C. O' Regan, P.R.F. Barnes, J.R. Durrant, J. Am. Chem. Soc. 131 (2009) 4808–4818.
[18] M. Grätzel, B. O'Regan, Nature 352 (1991) 737–740.
[19] J. Chen, J.L. Song, X.W. Sun, W.Q. Deng, C.Y. Jiang, W. Lei, J.H. Huang, R.S. Liu, Appl. Phys. Lett. 94 (2009) 153115.
[20] E. Guillén, F. Casanueva, J. Anta, A. Vega-Poot, G. Oskam, R. Alcántara, C. Fernández-Lorenzo, J. Martín-Calleja, J. Photochem. Photobiol. A: Chem. 200 (2008) 364–370.
[21] J. Kroon, N. Bakker, H. Smit, P. Liska, K. Thampi, P. Wang, S. Zakeerudin, M. Grätzel, A. Hinsch, S. Hore, U. Würfel, R. Sastrawan, J. Durrant, E. Palomares, H. Pettersson, T. Gruszecki, J. Walter, K. Skupien, G. Tulloch, Prog. Photovol.: Res. Appl. 15 (2007) 1–18.
[22] W. Lee, H. Okada, A. Wakahara, A. Yoshida, Ceram. Int. 32 (2006) 495–498.
[23] Z.S. Wang, Y. Cui, K. Hara, Y. Dan-Oh, C. Kasada, A. Shinpo, Adv. Mater. 19 (2007) 1138–1141.
[24] Z.S. Wang, Y. Cui, Y. Dan-Oh, C. Kasada, A. Shinpo, K. Hara, J. Phys. Chem. C 112 (2008) 17011–17017.
[25] D. Stockwell, Ye Yang, J. Huang, C. Anfuso, Z. Huang, T. Lian, J. Phys. Chem. C 114 (2010) 6560–6566.
[26] J.M. Rehm, G.L. McLendon, Y. Nagasawa, K. Yoshihara, J. Moser, M. Grätzel, J. Phys. Chem. 100 (1996) 9577–9578.
[27] R.R. Frontiera, J. Dasgupta, R. Mathies, J. Am. Chem. Soc. 131 (2009) 15630–15632.
[28] E. Hao, N.A. Anderson, J.B. Asbury, T. Lian, J. Phys. Chem. B 106 (2002) 10191–10198.
[29] H.N. Ghosh, J.B. Asbury, T. Lian, J. Phys. Chem. B 102 (1998) 6482–6486.
[30] I. Kondov, M. Čížek, C. Benesch, H. Wang, M. Thoss, J. Phys. Chem. C 111 (2007) 11970–11981.
[31] M. Giannouli, G. Syrrokostas, P. Yianoulis, Prog. Photovol.: Res. Appl. 18 (2010) 128–136.
[32] M.K. Nazeeruddin, A. Kay, I. Rodicio, R. Humphry-Baker, E. Muller, P. Liska, N. Vlachopoulos, M. Gratzel, J. Am. Chem. Soc. 115 (1993) 6382–6390.
[33] G. Smestad, Sol. Mater. 55 (1998) 157–178.
[34] F. Pichot, R. Pitts, B. Gregg, Langmuir 16 (2000) 5626–5630.
[35] Y. Liu, H. Wang, H. Shen, W. Chen, Appl. Environ. 87 (2010) 436–441.
[36] B. van der Zanden, A. Goossens, J. Phys. Chem. B 104 (2000) 7171–7178.
[37] V. Shklover, M.K. Nazeeruddin, S.M. Zakeeruddin, C. Barbe, A. Kay, T. Haibach, W. Steurer, R. Hermann, H.U. Nissen, M. Gratzel, Chem. Mater. 9 (1997) 430–439.
[38] G. Syrrokostas, M. Giannouli, P. Yianoulis, Renew. Environ. 30 (2009) 1759–1764.
[39] H.P. Lu, C.-Y. Tsai, W.N. Yen, C.-P. Hsieh, C.-W. Lee, C.-Y. Yeh, E.W.G. Diau, J. Phys. Chem. C 113 (2009) 20990–20997.
[40] H.-P. Lu, C.-L. Mai, C.-Y. Tsia, S.-J. Hsu, C.-P. Hsieh, C.-L. Chiu, C.-Y. Yeh, E.W.G. Diau, Phys. Chem. Chem. Phys. 11 (2009) 10270–10274.
[41] M. Fakis, V. Giannetas, J. Mikroyannidis, Dyes Pigments 87 (2010) 44–48.
[42] I.A. Trantakis, M. Fakis, S.S. Tragoulias, T.K. Christopoulos, P. Persephonis, V. Giannetas, P. Ioannou, Chem. Phys. Lett. 485 (2010) 187–190.
[43] L. Zeng, S. Dai, W. Xu, K. Wang, Plasma. Sci. Trans. 9 (2006) 172–175.
[44] R. Rao, V. Dutta, Nanotechnology 19 (2008) 445712–445721.
[45] M.K.I. Senevirathne, P.K.D. Pitigala, V. Sivakumar, P.V.V. Jayaweera, A.G.U. Perera, K. Tennakone, J. Photochem. Photobiol. A: Chem. 195 (2008) 364–367.
[46] H. Tributsch, Coordin. Chem. Rev. 248 (2004) 1511–1530.
[47] C. Longo, J. Freitas, M.A. De Paoli, J. Photochem. Photobiol. A: Chem. 159 (2003) 33–39.
[48] F. Zhang, J. Zhao, L. Zang, T. Shen, H. Hidaka, E. Pelizzetti, N. Serpone, J. Mol. Catal. A 120 (1997) 173–178.
[49] T. Wu, G. Liu, J. Zhao, H. Hidaka, N. Serpone, J. Phys. Chem. B 102 (1998) 5845–5851.
[50] B. Macht, M. Turrion, A. Barkschat, P. Salvador, K. Ellmer, H. Tributsch, Sol. Mater. 73 (2002) 163–173.
[51] K. Keis, C. Bauer, G. Boschloo, A. Hagfeldt, K. Westermark, H. Rensmob, H. Siegbahn, J. Photochem. Photobiol. A: Chem. 148 (2002) 57–64.
[52] D.W. Bahnemann, Israel J. Chem. 33 (1993) 115–136.
[53] M. Fakis, E. Stathatos, G. Tsigaridas, V. Giannetas, P. Persephonis, J. Phys. Chem. C 115 (2011) 13429–13437.
[54] J.B. Asbury, E. Hao, Y. Wang, H.N. Ghosh, T. Lian, J. Phys. Chem. B 105 (2001) 4545–4557.